

Creating multiple time-shared laser traps with simultaneous displacement detection using digital signal processing hardware

William H. Guilford,^{a,b,*} Joshua A. Tournas,^b Dragos Dascalu,^a and Douglas S. Watson^a

^a Department of Biomedical Engineering, University of Virginia, Charlottesville, VA 22908, USA

^b Department of Internal Medicine, Yale-New Haven Hospital, New Haven, CT 06510-3202, USA

Received 31 July 2003

Abstract

We present a design for implementing multiple laser traps for single-molecule studies through time-sharing using commercially available digital signal processing hardware in a computer running a standard multitasking operating system. This design enables four to six independent laser traps with a visitation frequency of $10,000 \text{ s}^{-1} \text{ trap}^{-1}$ and a timing jitter of $\pm 0.5 \mu\text{s}$ to be created. The design also achieves nanometer-resolution detection of displacement in all of the traps simultaneously via back focal-plane interferometry and only a single quadrant photodiode detector. Practical design considerations and limitations together with the use of fiberlasers in laser traps are discussed. Using this device, the mechanokinetics of multiple molecular motors or adhesion proteins may be measured simultaneously. We present the example biological application of two kinesin-coated beads in separate traps moving on different portions of a microtubule.

© 2004 Elsevier Inc. All rights reserved.

Keywords: Laser tweezers; Back focal-plane interferometry; Single-molecule studies; Kinesin; Multitasking

Applications of laser traps to cell biology and biophysics have been diverse. Chief among these applications is the use of laser traps to measure the mechanics of single macromolecules [1,2]. Such use is made possible by laser traps behaving as Hookean springs over short distances and by the use of an assortment of techniques for measuring minute displacements of objects within laser traps [3]. Laser traps may thus be used as molecular-level “spring scales” to assess displacement under load.

Oftentimes multiple laser traps are needed in a single field of view. For example, in the study of actin–myosin interactions, a “three-bead” system is typically used [1] in which two microspheres are held in independent laser traps and an actin filament is slung between them. This assembly is lowered onto a myosin-coated “pedestal” bead. The active myosin molecule attaches to and pulls

on the actin filament, which in turn displaces the microspheres in their respective traps. The use of two microspheres to hold and position the actin filament eliminates slack in the filament and restricts its Brownian motion.

There are two basic techniques for creating multiple laser traps in a single field of view. One approach is to physically split the original laser beam into two beams and recombine them at different angles into the back aperture of the microscope objective [1,4]. While simple and inexpensive to implement, these “split-beam” laser traps lack versatility in that they are generally limited to two laser traps. Furthermore, the only practical method to eliminate one of the traps is to physically block it, with the subsequent loss of that laser power.

An alternative approach is to “time-share” a single laser beam between two or more points in the focal plane using some mechano-optical or acousto-optical mechanism to deflect the laser beam [3,5,6]. Between laser “visitations,” each trapped microsphere diffuses

* Corresponding author. Fax: 1-804-982-3870.

E-mail address: guilford@virginia.edu (W.H. Guilford).

freely, but because microspheres in water are overdamped, if the laser visits each trap location sufficiently often, the trapped microspheres will not diffuse an appreciable distance between laser visitations. Time-sharing has the benefit of being optically simple (having a single light path, rather than two or more) and very versatile. The number and position of traps may be changed under computer control while preserving the total power.

For simple manipulation of cells or other trapped objects, the time-sharing approach is easily implemented [5]. In those instances, rates on the order of 10^3 visitations per second per trap are adequate. However, for precision work such as the molecular motor studies described above, implementation of the position switching system can be problematic. Modern computers, despite their blinding processor speeds, are limited by their operating systems in the speed and regularity with which they interact with peripherals. For example, an optimized C++ program running under Windows NT can update parameters on an I/O-mapped PCI card at rates around 4000 s^{-1} . However, to keep the mean microsphere diffusion distance between visitations to less than 1 nm, each trap must be visited by the laser $\sim 10,000\text{ s}^{-1}$. Making matters worse is that modern operating systems multitask and assign individual tasks to the CPU on a time-shared basis. When controlling a peripheral, the result is “jitter”—the timing variation from transition to transition in a signal. Consistent timing of position-to-position deflection of the laser beam is vital to creating multiple, stable traps by time-sharing. Yet jitter in accessing peripherals under multitasking operating systems may occasionally spike to hundreds of milliseconds.

There are two approaches to solving the combined problems of speed and timing in computer control of laser traps. Molloy [6] developed custom computer hardware to read proscribed trap positions from a pair of host computer memory locations, thus circumventing the operating system for actual position changes. A second approach is to use a “real-time” operating system, such as MS-DOS 6 or real-time Linux [7], that does not engage in multitasking. In interrupt-disabled or real-time operating systems, switching rates are limited by bus-addressing speed to $\sim 20,000$ position changes per second [3]—sufficient for two traps.

For studies of molecular mechanics, one must be able to measure the absolute position of a trapped object (or position relative to the center of the laser trap) with nanometer resolution. Early experiments with dual laser traps restricted detection of position to only one of the two traps. Since then, a number of research groups have used prisms to project images of two independently trapped beads onto separate quadrant photodiodes

(QP)¹ to measure their individual displacements [8,9]. This unfortunately requires rather clumsy optomechanics to align both quadrant photodiodes with their respective traps and is effectively limited to the case of two traps.

We here present a design for implementing time-shared laser traps using commercially available digital signal processing (DSP) hardware in a computer running a multitasking operating system. This enables four to six independent laser traps with a visitation frequency of $10,000\text{ s}^{-1}\text{ trap}^{-1}$ to be created. The design also achieves nanometer-resolution detection of displacement in all of the traps simultaneously via back focal-plane interferometry (BFPI) using only a single quadrant photodiode detector.

Materials and methods

A schematic of our laser trap system is shown in Fig. 1. There have been numerous articles and books published on the operational theory and construction of simple laser traps (e.g., [10,11]) to which the reader is referred. We will not here review the basics of laser trap design.

Lasers

The light source for the apparatus was a fiber laser (SDL FL-10; TEM₀₀, 11 W, 1112 nm). Fiber lasers used a doped, end-pumped fiber optic cable as the lasing medium. This results in high-CW power in a small package, with near perfect beam quality. While not specifically reported by the manufacturer, we measured the short-term (<10 s) pointing stability to be approximately $15\text{ }\mu\text{rad}$. This measurement was done by bolting the laser head and a duolateral position sensing device (OnTrak Photonics) exactly 1 m apart on an optical breadboard, sealed against air currents in an elongated box. Incident power during this measurement was reduced to a subsaturating level using a reflective neutral-density filter. The position of the beam was determined using a normalizing amplifier (OnTrak Photonics).

Cooling fans in the fiber laser caused significant interference centered at 120 Hz, despite the isolation of having the light emitted from a single-mode fiber. We eliminated this noise by disabling the cooling fans and connecting the laser to the building air exhaust system with flexible plastic ducting (6-in. diameter).

¹ Abbreviations used: DSP, digital signal processing; LEMs, longitudinal electromagnetic modes; AOD, acousto-optic deflector; BFPI, back focal-plane interferometry; QP, quadrant photodiode; A/D, analog-to-digital; D/A, digital-to-analog; DMA, direct memory addressing; IP, Industry Pak; GUI, graphical user interface; Pipes, 1,4-piperazanedithanesulfonic acid; OS, operating system.

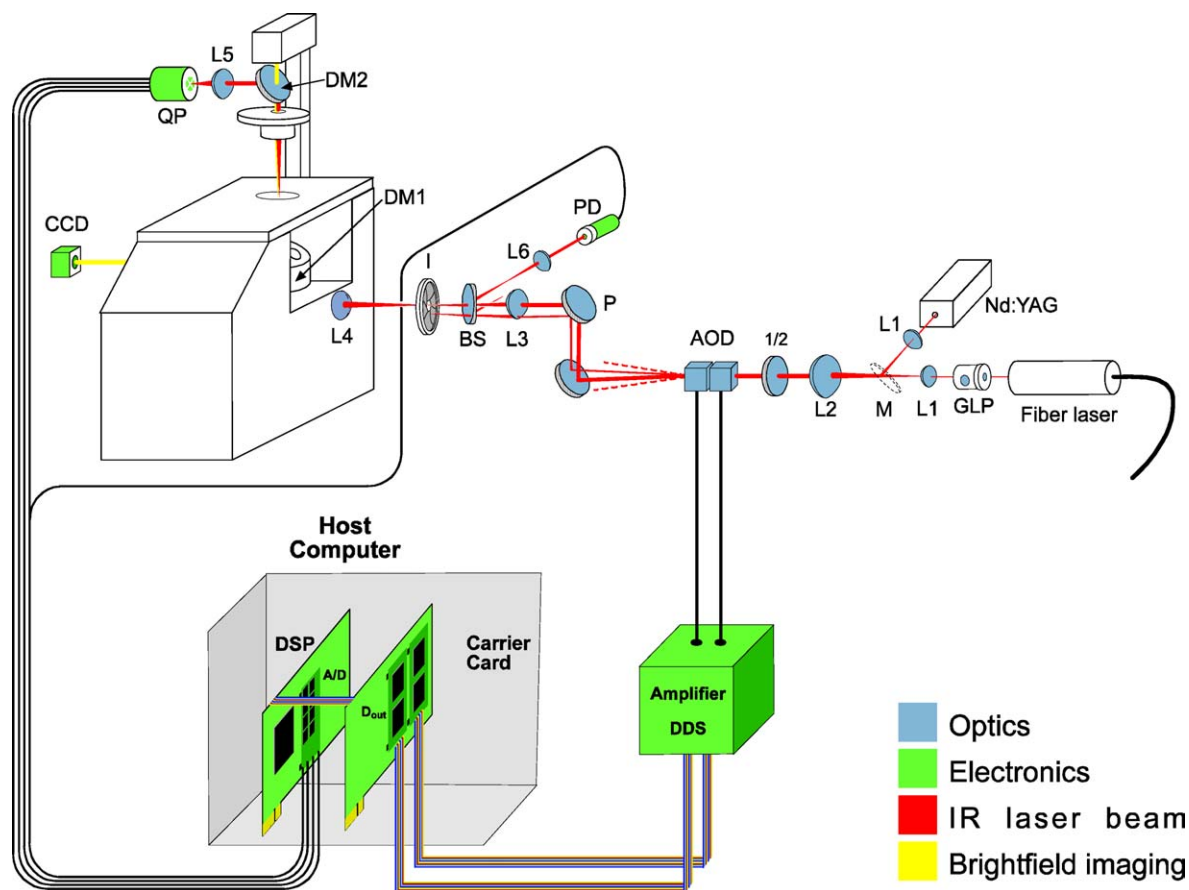


Fig. 1. Schematic of the laser trap. FL, fiber laser; Nd:YAG, Nd:YAG laser; GLP, Glan laser prism; Lx, lenses; M, removable mirror; 1/2, half-wave plate; AOD, acousto-optic deflector; P, periscope; BS, beam sampler; PD, photodetector; I, iris diaphragm; DMx, dichroic mirrors; QD, quadrant photodiode; CCD, charge-coupled device camera; DSP, digital signal processing card; A/D, analog-digital converter; D_{out}, digital output cards; DDS, direct digital synthesis subsystem.

For comparison, a low-cost Nd:YAG laser (ISF064-1000, Intelite; 1 W, TEM_{0,0}, M² = 1.15, 1064 nm) was mounted orthogonal to the optical axis, between the two lenses of the first beam expander. The emitted beam could replace that from the fiber laser via a mirror in a flip-up optical mount (New Focus). Pointing stability of this laser is <50 μrad.

Polarization and noise issues

Many fiber lasers have randomly polarized outputs—that is, the emitted light consists of a large number of closely spaced longitudinal electromagnetic modes (LEMs), each with its own polarization. By in large, these LEMs cluster into two orthogonal groups. While the average power of the beam may remain relatively constant, the power randomly switches from one set of polarizations to the other. This is a result of birefringence and hole burning (addressed in the Discussion). If the beam is to be polarized as required by our acousto-optic deflector (AOD), it is beneficial to select light at a polarization of 45° to each of these axes. This greatly reduces the power fluctuations that are passed on to the specimen plane.

The fiber laser was mounted in a custom holder made from aluminum. A Glan laser prism was mounted in a rotary stage immediately in front of the laser aperture (GL in Fig. 1). An InGaAs photodetector was temporarily placed beyond the prism (NewFocus; 2011-FC) and connected to an oscilloscope. The Glan laser prism was rotated to minimize power fluctuations. As expected, this angle was 45° from vertical and 45° in each direction from peak power representing the orthogonal axes of the LEMs. A 1/2 wave plate was placed after the first beam expander to return the beam polarization to vertical. It was rotated to achieve maximum diffraction efficiency during alignment. Reflected energy from the Glan prism was dumped into a firebrick. This entire operation results in the loss of slightly more than 50% of the emitted laser power.

Beam expanders and beam deflection

A basic requirement for a stable laser trap is that the laser beam be expanded to slightly overfill the back aperture of the microscope objective. However, in the case where multiple laser traps are created using the

technique of time sharing [3,6], there are additional considerations in choosing the power and placement of beam expanders to achieve this.

Multiple laser traps are created in a single field of view by varying the angle at which a laser beam (or multiple laser beams) enters the back aperture of the microscope objective. The change in lateral position of the laser trap in the focal plane is given by the product of the angular deflection (θ) and the effective focal length (f_e).

$$d = f_e \theta, \quad (1)$$

f_e is not the same as the working distance and must usually be obtained from the objective manufacturer; 1.8 mm is a typical f_e value for high-numerical-aperture objectives, including that used here (Olympus UPLFL 1.3 n.a., 100 \times).

Eq. (1) sets an upper limit on the lateral separation of two laser traps, given a maximum θ that can be generated by the deflection optics. There is, of course, a maximum range of angles ($\Delta\theta_{\max}$) that can be accepted by an objective. $\Delta\theta_{\max}$ can be estimated as

$$\Delta\theta_{\max} \approx f_{\#}/m \cdot f_e, \quad (2)$$

where m is the magnification of the objective and $f_{\#}$ is the field number of the objective (22 mm for current Olympus objectives). For example, the above objective would be expected to accept light entering over a 0.12-rad (7°) range or up to 0.06 rad off the optical axis. While some mirror- or lens-based deflection systems may be able to reach this limit, most time-shared laser traps will rely on the speed of an acousto-optic deflector, and these devices cannot ordinarily generate such large deflections.

AODs use ultrasound traversing a crystal to create a virtual diffraction grating for entering laser light. The angle of deflection (θ) for the first-order diffracted spot is dependent upon the wavelength of the laser light in the diffraction medium (λ) and the acoustic wavelength within the medium (v_a),

$$\theta = \lambda/v_a, \quad (3)$$

The maximum range of deflection angles (θ_{\max}) that can be generated is given by

$$\theta_{\max} \leq \lambda f_b/v_a, \quad (4)$$

where λ for our fiber laser is 1112 nm, f_b is the acousto-optic bandwidth (7 MHz for our AOD), and v_a is 617 m/s for tellurium oxide crystals in shear. In our system, this gives a maximum deflection range of 0.013 rad (0.7°). By Eq. (1), this translates to a deflection of 23.4 μ m in the specimen plane. This is the theoretical maximum separation of two traps that may be generated using this AOD.

In practice, this degree of separation is seldom achieved. AODs have a maximum optical aperture in which an incident laser beam will be diffracted. Stock AODs will typically accommodate a beam 3–5 mm in

diameter. The limitations on the diameter of the optical aperture are twofold: (1) manufacturing cost and (2) response time. The maximum rate at which an AOD may change diffraction angles is determined by the time required for the acoustic signal to propagate across the width of the beam. For example, a typical aperture size of 3 mm gives a response time of 4.9 μ s. This is much faster than the dwell time typical of a time-shared laser trap (50 μ s)—that is, the amount of time spent at each trap location.

However, because we must fill or overfill the back aperture of the microscope objective, typically 6 mm in diameter, the beam must be expanded $>2\times$ after diffraction for a 3-mm AOD aperture. Beam expanders reduce angular changes by the degree of expansion. Thus, Eq. (4) becomes

$$\theta_{\max} \leq \frac{A_{\text{AOD}}}{A_O} \cdot \frac{\lambda f_b}{v_b}, \quad (5)$$

where A_O and A_{AOD} are the apertures of the objective and the AOD, respectively. This will obviously translate into a decrease in the lateral separation of laser traps. Thus, it is obviously beneficial to use an AOD with an optical aperture approximating the diameter of the objective back aperture. Unfortunately, this both results in an increase in cost and may limit the number of simultaneous traps (N) or the frequency at which one may switch between them (f_s).

As multiple traps are created, the dwell time of the laser beam at any given trap will fall. The dwell time (t_d) will be

$$t_d = \begin{cases} \infty, & N = 1, \\ \frac{1}{N \cdot f_s} - \frac{A_{\text{AOD}}}{v_a}, & N > 1, \end{cases} \quad (6)$$

where A_{AOD}/v_a is the “fill time” or the amount of time required for ultrasound to transit the aperture. This is similar to the expression given by Visscher and Block [3]. We used a two-axis TeO_x AOD (NEOS) with a 6-mm optical aperture. The extended fill time of our large aperture ($\approx 10 \mu$ s) obviously prohibits generating 10 simultaneous traps at a 10,000 visitations s^{-1} trap $^{-1}$, as the effective dwell time will be zero. It is intuitively obvious that trap stiffness will vary in direct proportion to dwell time for a given laser power.

The 6-mm aperture required that the beam be expanded slightly after the AOD. We incorporated 10% beam expansion into an “afocal” system of lenses that causes angular deflections of the laser beam about the center of the AOD to be translated into corresponding angle-of-incidence changes at the objective back aperture, as shown by Fällman and Axner [5]. Were such a system of lenses not used, the beam would sweep laterally across the back aperture by a distance $D\theta$, where D is the distance of the AOD from the objective.

The beam expander consisted of a lens mounted to the laser port on our Olympus IX70 microscope (L4 in

Fig. 1). The focal length of this second lens was chosen to be equal to the length of the light path from the laser port to the objective. The focal length of the first lens (L3) was chosen to approximate the proper expansion ($M2 = 1.16X$) given by the equation $f_{L3} = f_{L4}/M2$. All the other optical components were adjusted so that L3 was a distance $f_{L3} + f_{L4}$ from the microscope and the midpoint of the AOD was a distance f_{L3} from L3. This expander reduced the theoretical maximum lateral excursion of the trap to 20.1 μm .

The first beam expander, before the AOD, was fashioned to expand the laser beam ($1/e^2$ diameter 0.43 mm) to the AOD aperture diameter (6 mm). All lenses were antireflection coated (Newport Corp., AR18).

Back focal-plane interferometry

Others have described the technique BFPI [12,13]. In brief, BFPI uses forward-scattered light from a trapped object to monitor its position within the diffraction-limited focal point. The light from the trapping laser or a secondary detection laser is collected by the microscope condenser, and an image of the condenser back focal plane (BFP) is projected with appropriate magnification onto a quadrant photodiode or linear position sensor [14].

In a time-shared laser trap, it should be possible to monitor the position of every trapped object within their independent traps by this technique. The forward-scattered light originates from a single trap position at any point in time. Thus, if the detector is sufficiently fast and data collection is synchronized with beam deflection, one may monitor the position of all trapped objects simultaneously.

Traditionally, silicon QPs are used in BFPI. Unfortunately, silicon photodiodes are approximately 1/100 as sensitive in the near infrared as at their peak wavelengths (500–600 nm). This necessitates large current–voltage converter gains, increases noise, and reduces bandwidth.

In recent years germanium QPs have become available (Judson Technologies). Germanium photodiodes are not only extremely sensitive in the near IR but are nearly insensitive to visible wavelengths. Thus, less gain is required for a germanium compared to a silicon GP, keeping the bandwidth high.

We incorporated a 3-mm germanium QP (Judson Technologies) into a custom holder that mounts in place of the DIC prism in an Olympus condenser that holds a microscope objective (Leitz 40X; na 0.65, O2 in Fig. 1) as the condenser. The custom mount also contains a dichroic identical to that in the laser port, reflecting forward-scattered light from the BFP. The BFP is imaged onto the QP by a lens (L5). A pair of one-dimensional linear translation stages allows fine alignment of

the QP. The assembly was designed using parametric CAD (Autodesk Mechanical Desktop) to properly position the lens based on the distances to the QP and the BFP based on available lenses and aperture diameters.

Uncalibrated X and Y positions of the trapped object are calculated as usual,

$$X = \frac{(A - C) + (B - D)}{P} \quad \text{and} \quad (7)$$

$$Y = \frac{(A - B) + (C - D)}{P},$$

where $A \dots D$ designate the voltage output from each quadrant amplifier and P is a measure of the laser power (discussed below).

In principle one can digitize the output of each quadrant and determine these positions numerically. However, the output of each quadrant consists of a small signal superimposed upon a large DC offset. Unless the analog-to-digital (A/D) converters are of particularly high resolution (>16 bits), unacceptable quantization noise will result. Given the relative scarcity and long conversion times of such A/D converters, we chose instead the more traditional route of constructing an “analog computer” to perform these calculations, similar in most respects to those described by others [1,15]. The frequency-limiting component in such systems is generally the analog divider. Fortunately, high-bandwidth analog dividers (10 MHz) are now available (AD734) and were used in our construction. Differences in Eq. (7) were performed first to minimize common mode effects.

We introduced a wedge beam sampler (Newport) between the two lenses of the second beam expander, downstream of the AOD. This deflected a fraction ($\approx 5\%$) of the beam into a 2-cm length of multimode optical fiber coupled to an InGaAs photoreceiver (NewFocus 2011-FC, 200 kHz bandwidth). By placing the photoreceiver at the focal point of an intermediate 50-mm lens, L6, the sampled beam entered the fiber regardless of AOD deflection angle yet did not saturate the detector and thus represented the laser power incident at the specimen plane. The output of the photoreceiver could be used to normalize the QP signals, as in Eq. (7). This measure of incident power was similarly effective in normalizing against variations in laser power as is the sum of all quadrants ($A + B + C + D$) for static trap positions, save for a small degree of interference from the dichroic mirror.

All optics were mounted on 1-in.-diameter stainless steel pedestals (NewFocus), translation stages (Newport) and in standard optics mounts except where otherwise indicated.

Digital hardware

To circumvent delays and jitter introduced by computer operating systems, we programmed a DSP board

to control the AOD and simultaneously collect data from the QP. DSP chips are essentially reduced-instruction set microprocessors specialized for performing mathematical operations common in signal processing applications. Available from a variety of manufacturers (e.g., Texas Instruments, Motorola), they can also be purchased on expansion boards with a number of bus architectures (PCI, ISA, VME) and include memory and bus interface chips. The characteristics that make DSP cards ideal for this type of application are (1) real-time operation and lack of operating system, which reduce jitter, (2) optimization for floating-point operations, and (3) ability to directly address A/D inputs, D/A outputs, digital outputs, and the host computer memory. The disadvantage of using DSP cards is that two programs must typically be written: one that operates the instrumentation and resides on the DSP card and one that provides a user interface and resides on the host computer.

We utilized a TI 340C40-based DSP card for PCI bus (Dakar, Spectrum Signal Processing) running at 66 MHz, with 512k memory and direct memory addressing (DMA). This card was installed in a Pentium III microcomputer (Dell Optiplex GX110), along with an Industry Pak (IP) carrier card (Imola, Spectrum Signal Processing). The two cards were connected using a high-speed 32-bit interconnect (DSP-link3). A pair of 32-bit parallel digital output cards (TEK Microsystems, FP-Parallel32) were installed on the carrier card, and a 100-kHz, 16-bit, parallel 4-A/D, 2-D/A I/O card (DL3-A1, Spectrum Signal Processing) was installed on the DSP card.

The 32-bit digital output cards were used to drive the independent channels of a combined direct digital synthesis sine-wave generator and RF amplifier (NEOS). This drives the AOD at a center frequency of 37 MHz.

The A/D converters collect data from the QP, and select traps are echoed on the D/A converters for display on a color digital oscilloscope (Tektronix). In addition to the DSP and carrier cards, the computer also hosts a high-voltage driver that controls a three-dimensional piezoelectric microscope stage (Nanonics Inc., Israel).

Host program/GUI

An application on the host computer serves as an interface between the user and the DSP board. Written in Microsoft Visual C++, GUI provides controls to activate any of up to six traps, save data, control trap locations and the position of the piezoelectric stage control. The host computer also serves as storage for DSP-collected data. Windows NT typically maintains most of the available memory in a “paged” state; thus the memory contents may be dynamically swapped to a “paging file” on the hard drive. Paged memory is not PCI bus-accessible. We increased and fixed the amount of PCI-accessible

(nonpaged) memory by setting the Windows NT system registry key: HKey_Local_Machine\System\CurrentControlSet\Control\SessionManager\MemoryManagement\NonPagedPoolSize.

The default value (0) of this entry means that the operating system will automatically calculate a value. One may set this value to anything less than 75% of the total amount of RAM in the computer. We operate with a NonPagedPoolSize of 0x3200000 (50 MB). This is adequate to store over 240 s of data at 10,000 samples/s from a single trap with both *X* and *Y* axis displacement data.

A simplified flow diagram of the host program and its interactions with the DSP card is shown in Fig. 2. The host program first allocates PCI-accessible memory (using a library function supplied by the DSP card manufacturer) for two items: (1) a small “shared array” for passing data and commands between the DSP card and the host and (2) a large block of memory for data accumulation. The DSP card is reset, and the locations of these two allocated memory blocks are loaded into “PCI mailboxes,” which are registers implemented on many PCI cards for host-card communication. In this way the host “informs” the DSP card of the locations where it should send and retrieve data. The host program then loads the DSP program onto the board, which starts immediately.

Whenever the user changes a basic parameter, such as the desired number or locations of laser traps, updated control values are passed to the DSP card through the aforementioned shared array. This array is the heart of the host–DSP interface. The exact order and contents of the array is given in Table 1, which includes the number and locations of the laser traps, and flags for data collection. Updated values are written to the PCI-accessible location previously set aside for the array and asynchronously collected by the DSP card (see below).

It is evident that the DSP-based program, described below, handles virtually all aspects of trap creation and data collection. The host program is idle most of the time and simply responds to GUI or mouse events. In fact, if the host program terminates abnormally, the DSP card continues to generate the last-indicated number of traps.

Two time-critical and often simultaneous activities are handled by multithreading: stage control and data collection. A driver card in the computer controls the piezoelectric microscope stage. It is often the case that a preprogrammed stage movement (such as a constant velocity, back-and-forth movement) is taking place at the same time as data collection. During data collection by the DSP card, the host must check for a “collection done” flag in one of the PCI mailboxes in a timely fashion or program crashes result. While neither of these processes is especially processor intensive, they are both time critical. Both are easily handled by spawning separate “worker threads” under the Windows NT API. This highlights an advantage to using a multitasking environment rather than a real-time operating system.

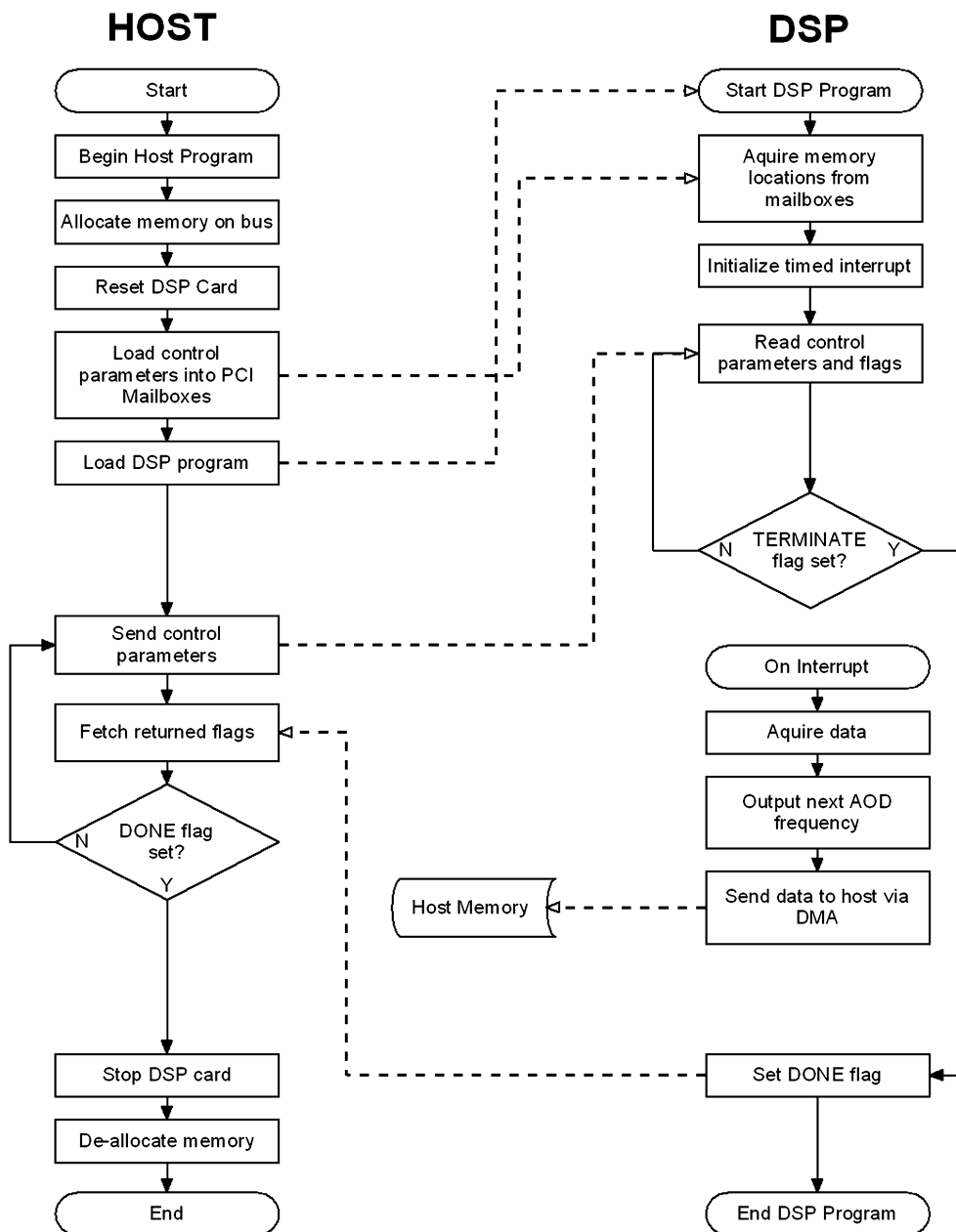


Fig. 2. Simplified flow diagram of the host computer and DSP programs. Communications between the programs and the hardware are shown in dashed lines. Details are given in the text.

Program termination is by passing a TERMINATE flag to the DSP card through a PCI mailbox. The host program waits while the command is processed, and a DONE flag returned to the host signals termination of the DSP program. The host program then stops the DSP card, deallocates the nonpaged memory, and terminates normally.

DSP program

The DSP program launches when loaded to the DSP card by the host and proceeds through a series of initialization routines. These include acquiring the location

and size of the available host memory block from the “PCI mailboxes,” which are registers implemented on many PCI cards for host–card communication. The DSP also acquires from a mailbox the location of the “shared array” containing the number and location of the laser traps (detailed below).

A timed interrupt is set, with the interval between interrupts set equal to the inverse of the product of the number of traps and the visitation frequency. The default values for these two parameters are one trap and 10 kHz, respectively, resulting in an interrupt interval of 10⁻⁵ s. On each timed interrupt, the DSP acquires the position data for trap *n* – 1 from the A/D channels.

Table 1
Order and contents of the shared array

Cell	Variable	Description
0	T1_COLLECT	Flag to collect data from trap 1
1	T1_ANALOG1	Echo data from trap 1 to analog output 1?
2	T1_ANALOG2	Echo data from trap 1 to analog output 2?
3	T1_X_POSITION	X-axis AOD frequency for trap 1
4	T1_Y_POSITION	Y-axis AOD frequency for trap 1
5	T2_COLLECT	Trap 2...
6	T2_ANALOG1	
7	T2_ANALOG2	
8	T2_X_POSITION	
9	T2_Y_POSITION	
10	T3_COLLECT	Trap 3...
11	T3_ANALOG1	
12	T3_ANALOG2	
13	T3_X_POSITION	
14	T3_Y_POSITION	
15	T4_COLLECT	Trap 4...
16	T4_ANALOG1	
17	T4_ANALOG2	
18	T4_X_POSITION	
19	T4_Y_POSITION	
20	T5_COLLECT	Trap 5...
21	T5_ANALOG1	
22	T5_ANALOG2	
23	T5_X_POSITION	
24	T5_Y_POSITION	
25	T6_COLLECT	Trap 6...
26	T6_ANALOG1	
27	T6_ANALOG2	
28	T6_X_POSITION	
29	T6_Y_POSITION	
30	NUMBER_OF_TRAPS	Number of traps currently enabled
31	SAMPLING_FREQUENCY	Sampling/switching frequency
32	COLLECTION_FLAG	Collect data now
33	ARRAY_COLLECTION_ADDRESS	Save data to this address
34	COLLECTION_TIME	Collect data for this length of time
35	IS_T1_ENABLED	Flag for trap 1 being enabled
36	IS_T2_ENABLED	Flag for trap 2...
37	IS_T3_ENABLED	Flag for trap 3...
38	IS_T4_ENABLED	Flag for trap 4...
39	IS_T5_ENABLED	Flag for trap 5...
40	IS_T6_ENABLED	Flag for trap 6...

The encoded frequencies for trap n are sent to their respective parallel digital output cards that in turn control the DDS. Data are acquired for the previous ($n - 1$) trap on each cycle. Waiting the duration of one interrupt before data collection allows time both for the QP

detector to settle after the laser is deflected and for one or more A/D conversion cycles to occur.

The most recently acquired data are echoed to the D/A output channels if echoing trap $n - 1$ is so indicated in the shared array. This allows the data to be displayed on an inexpensive digital oscilloscope, reducing the central processing unit load that would be caused by drawing to the computer screen. Finally, data for trap $n - 1$ are returned to the host into an incremented memory location via DMA.

Acquisition continues until terminated by the user or until a preset time limit is reached. Between interrupts, a PCI mailbox is repetitively checked for a flag indicating that data collection should begin or that the DSP program should terminate. When the TERMINATE flag is set, the DSP program prepares to end and returns a DONE flag through the mailbox immediately prior to termination.

Calibration and characterization

Jitter is defined as cycle-to-cycle variations in the timing of trap position transitions. The response time of the DDS is constant at 20 ns, and so does not contribute to jitter on our time scale. Thus, jitter was determined by monitoring a high-order bit on the digital output cards for the cycle-to-cycle variability in the timing of its state change. A digital oscilloscope (Tektronix) was triggered on the ascending limb of a state change (marking a change of AOD frequency), and the descending limb of the following state change (a return to the previous frequency) was monitored for variations in timing.

On-line power spectral density $S(f)$ was monitored using commercial software (AtSpec, Taquis.com) and a rectangular window function. Off-line $S(f)$ calculations and curve fitting were accomplished using software developed in Delphi (Borland) based on standard algorithms [16]. Trap stiffness α and QP sensitivity were determined by curve fits to $f^2 \cdot S(f)$, as described by Allersma et al. [13]. $f^2 \cdot S(f)$ reaches a plateau, P_V , above the corner frequency, f_0 , that is related to the detector sensitivity β (in units/m) by

$$\beta = (P_V d / 4.42 \times 10^{-20})^{1/2}, \quad (8)$$

where d is the diameter of the microsphere in meters. This plateau value may be measured directly from averaged spectra or extrapolated from curve fits. Based on the equations of Allersma et al. [13], one may easily show that in the limit of $f \rightarrow \infty$,

$$f^2 S(\infty) = P_V = S_0 f_0^2, \quad (9)$$

where S_0 is the magnitude of the spectrum at $f = 0$. Trap stiffness may be independently determined from f_0 by

$$\alpha = 6\pi^2 \eta d f_0, \quad (10)$$

A Lorentzian was fit to $S(f)$ using a simplex algorithm [16] and a least-squares estimator. Briefly, 16 to 64

nonoverlapping spectra were averaged and multiplied by f^2 . These data were then fit by the equation

$$f^2 S(f) = S_0 f_0^2 f^2 / (f_0^2 + f^2) \quad (11)$$

to find S_0 and f_0 . The fitted values are substituted into Eqs. (8)–(10) to find the QP sensitivity and trap stiffness. However, one need not take the product $f^2 \cdot S(f)$ to determine these values. $S(f)$ may be directly fit by

$$S(f) = S_0 f_0^2 / (f_0^2 + f^2). \quad (12)$$

Fitting Eq. (11) to the data emphasizes frequencies above f_0 and is best for determining QP sensitivity, while fitting Eq. (12) emphasizes frequencies at and below f_0 and is best for determining stiffness. They converge to the same values only in an ideal spectrum.

Laser trap observations of single kinesin molecules

Full-length *Drosophila* kinesin was a kind gift of William O. Hancock of Pennsylvania State University. All protein buffers consisted of 80 mM Pipes, 1 mM MgCl_2 , 1 mM EGTA, and 1 mM ATP (pH 6.84). Buffers were made fresh daily and thoroughly degassed under vacuum. Microtubule buffer also contained 20 μM taxol.

Glass coverslips (18 \times 18 and 22 \times 22 mm) were washed sequentially in detergent, 1 M HCl, and acetone for 5 min each and coated with 3-aminopropyltriethoxysilane. A flow chamber was created between the large and the small coverslips with 0.1-mm mylar spacers (PractiShim). They were attached with optical adhesive (Norland) and cured for 2 min in a UV oven. Approximate chamber volume was 10 μL .

Microtubules were assembled from bovine brain tubulin (cytoskeleton) as described by Hamel et al. [17]. Briefly, 4 μL solution containing 5 mg/mL rhodamine-labeled tubulin, 1 mM MgCl_2 , 1 mM GTP, 10% dimethyl sulfoxide, and 80 mM Pipes was incubated for 40 min at 37 $^\circ\text{C}$. Microtubules were immediately diluted 100-fold into microtubule buffer, described above. Assuming an average microtubule length of 5 μm , the final microtubule concentration was approximately 250 nM. Microtubules were stored at room temperature.

Kinesin-coated beads (0.6 μm silica, Bangs Labs) were exposed to silanized, microtubule-coated surfaces as described by Svoboda et al. [18]. Trap stiffness and QP calibration were determined by fits to power spectra as described earlier.

Results

Bandwidth, speed, and jitter

With a first-stage current–voltage gain of 10^3 V/A, each quadrant of the germanium QP had a 3-dB bandwidth of 420 kHz, measured with sinusoidal amplitude-

modulated light at 915 nm. The bandwidth of the subsequent components, including the analog divider, exceeds this bandwidth. Thus the lumped system bandwidth of the analog components was limited by the current–voltage conversion. The measured response of the system to a step in light intensity had a $(1 - 1/e)$ rise time of 1.7 μs . This extremely high bandwidth is due to the use of both a germanium QP rather than a silicon QP, and a fast (10-MHz) analog divider.

AOD frequency switching was limited to 6×10^4 frequency changes per second without data collection or 4×10^4 frequency changes per second during data collection. These rates are adequate for six and four simultaneous traps, respectively (at 10,000 visitations s^{-1} trap $^{-1}$). Piecewise deprecation of the DSP code revealed that the principle speed limitation was the initialization of each DMA transfer, into and out of the host memory. When DMA transfers were disabled and the desired frequencies hard-coded, we achieved a maximum frequency switching rate of 1.2×10^5 s^{-1} —well in excess of what can be achieved by the AOD.

Jitter was exactly ± 0.5 μs (± 0.35 μs RMS) at switching rates within the above-stated limits. Other tasks on the host computer (e.g., playing a CD, browsing the internet) do not affect jitter.

The aggregate rate of 4×10^4 frequency changes per second could be subdivided as desired among the traps (e.g., 4×10^4 s^{-1} for a single trap, or 2×10^4 s^{-1} trap $^{-1}$ for two traps) to give higher position sampling rates. This was accomplished by simply altering the number of traps and setting the interrupt frequency of the DSP to the appropriate value. At constant laser power, trap stiffness is expected to vary with dwell time (Eq. (6)) as the number of traps is increased. Indeed, measured trap stiffness was well fit by the predicted dwell time (Fig. 3). Fig. 3 (inset) also shows the uncalibrated response of the QP and analog computer to a deflection of the laser beam between two trap locations—one containing a bead (filled) and a second empty trap positioned well off the optical axis to give a clean response. The integration interval of the A/D converter is shown in gray. “Channel separation” between two traps was estimated based on cross-correlation [19] to be >44 dB (158-fold). Cross talk is generated principally in the analog computer and not in the DSP system or the A/D converter.

PSD and noise

Data for four simultaneously trapped 1- μm beads at 2 W laser power and 10^4 visitations s^{-1} trap $^{-1}$ were saved. Their individual power spectra are shown in Fig. 4 (upper traces in each frame). The classic Lorentzian shape is obvious in each of them. Deviations from ideal beginning at approximately 2.5 kHz and extending upward are apparent. This was due to the 10-kHz digital/optical sampling of bead positions within their traps,

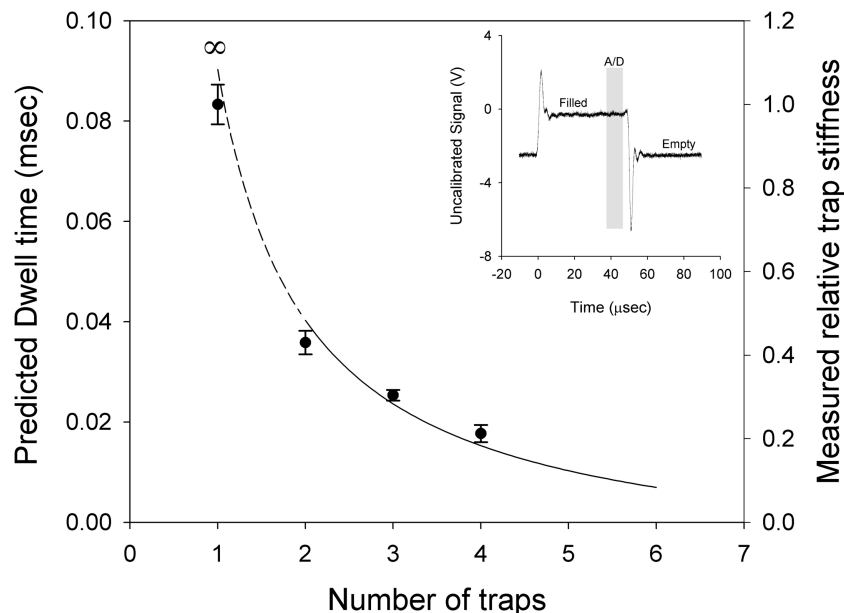


Fig. 3. Dwell time and trap stiffness versus number of active traps. Dwell time was predicted by Eq. (6), and for clarity is shown as a continuous function although it applies only at integer trap numbers. The actual dwell time with a single trap is ∞ , since position never changes, so the trend toward $N = 1$ is shown as a dashed line. Trap stiffness is shown normalized to a single trap. Error bars indicate \pm one standard deviation based on several trapped beads. (Inset) Uncalibrated signal from the analog computer when the laser is displaced from a filled trap (containing a bead) to an empty trap positioned significantly off axis. The gray bar indicates the maximum range of times over which this analog signal could be integrated by the A/D converter.

resulting in a Nyquist frequency of 5 kHz. Frequencies >5 kHz were aliased.

Spectra using empty traps (Fig. 4, lower traces in each frame) and a stationary microsphere using both lasers were also obtained. The fiberlaser exhibited increased noise at very low frequencies (<1 Hz) and high-frequency laser pump noise (>2 kHz) compared to the Nd:YAG laser. Nonetheless, both lasers typically yielded noise densities $<1 \text{ \AA Hz}^{-1/2}$ above 5 Hz. Stage drift 3.2 nm/min.

Beads could be trapped over a lateral expanse of 20 μm , approximating the maximum separation that we predicted based on the bandwidth of our AOD and our optics (20.1 μm ; Eq. (5)), though trap stiffness was markedly lower at the extrema. Stiffness varied 10% (RMS) between beads in four different traps. There was similarly 10% RMS variation between different beads in one of the four traps. Thus, variations in QP sensitivity and trap stiffness in the four traps were entirely explained by variations in the trapped beads. QP sensitivity varied 4% RMS between beads and decreased only slightly as the number of traps was increased from one to four without concomitant increases in laser power.

Biological example

Two 0.6- μm kinesin-coated microspheres were held in independent laser traps and brought into contact with different segments of a single fluorescently labeled microtubule to independently record single displacement events (Fig. 5). The stiffness of each trap was 0.0043–

0.0045 pN/nm. Less than half of all microspheres move on microtubules, suggesting single motor interactions [18]. “Staircase” events were observed asynchronously in the two traps, each showing decreasing noise with increasing excursion from trap center, along with single steps and slips at multiples of 8 nm. Pause time between steps averaged 21 ± 2 ms at 250 μM ATP and room temperature.

Discussion

Using DSP hardware to create multiple laser traps has distinct advantages over traditional approaches. The floating-point specialization of DSP processors and lack of OS overhead allows exceptional speed. Seamless integration with I/O expansion cards permits simple and fast interfacing with trap components, including the acousto-optic deflector and quadrant photodiode. This permits coordinated data sampling for simultaneous displacement detection regardless of number or position of the laser traps. Using DSP hardware also provides an off-the-shelf solution to developing laser trap control systems and allows one to use a host computer with a standard operating system.

Using DSP hardware, and our design in particular, does have some disadvantages. The first and most evident problem is in the complexity of programming involved. Two programs are required—one running on the DSP card and one on the host computer.

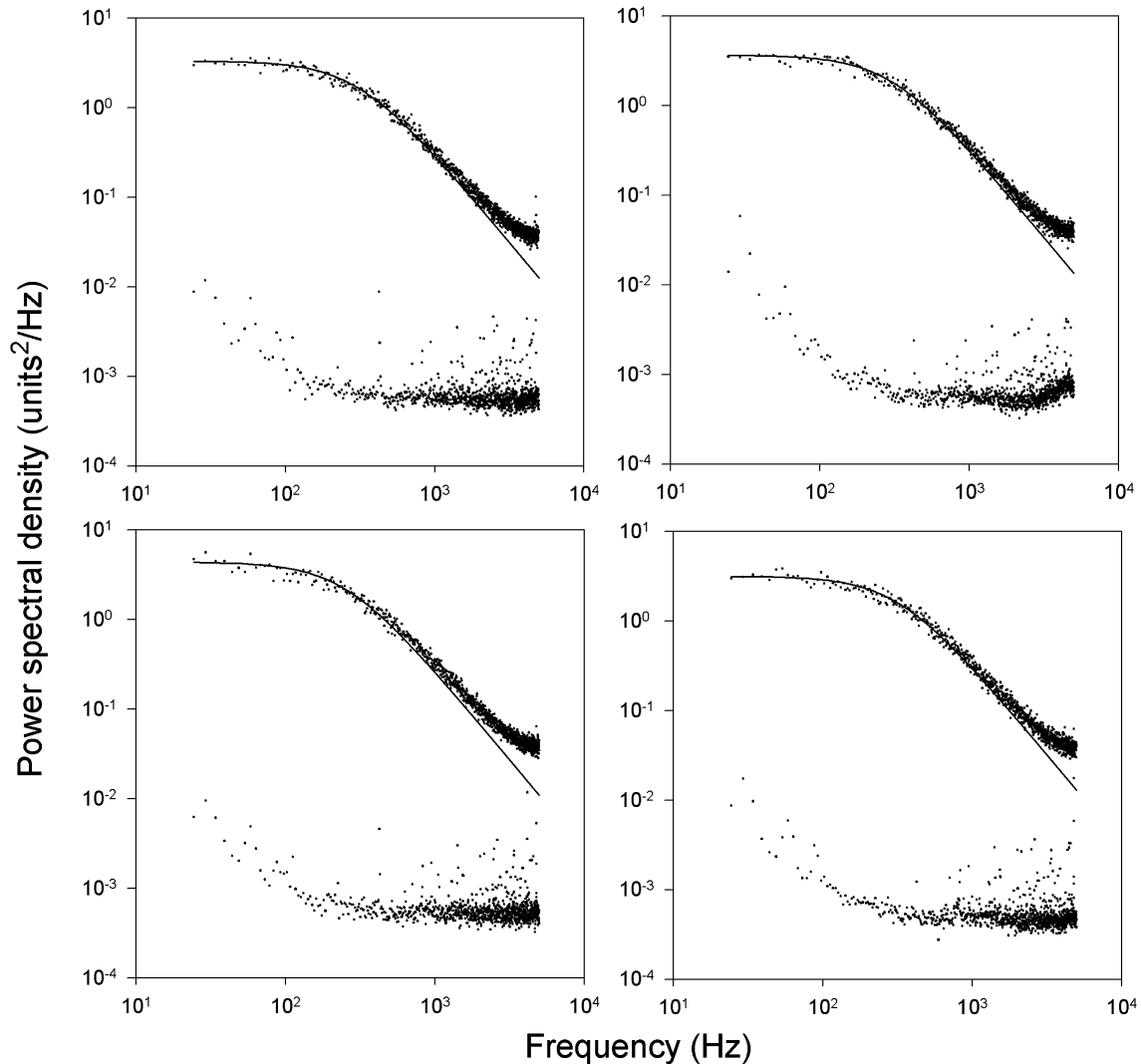


Fig. 4. Uncalibrated power spectra of multiple simultaneous laser traps separated laterally by approximately $5\ \mu\text{m}$ (arranged in a square along both axes) with and without a trapped $1\text{-}\mu\text{m}$ microsphere (upper and lower traces, respectively). Trap stiffness ranged from 0.015 to $0.019\ \text{pN/nm}$, which is similar to the variation in stiffness between randomly chosen microspheres. Lines show the best fit of Eq. (12).

These programs must integrate and communicate seamlessly. Variable types and numeric representations in particular are not always the same between the host computer, the DSP processor, and the add-on cards. Further, to achieve adequate performance much of the DSP program is written in assembly language. Developing the software for this type of system is therefore quite challenging.

Our detection method prohibits doing straightforward force-feedback on a single trap. Feedback control of trap position can be used to hold a trapped microsphere stationary under an applied load [1]. However, proper feedback control requires integration of the “error signal”—the difference between the actual and the desired absolute microsphere position. This can be done when position detection is independent of the trapping laser [3]. But when the trapping laser is integral to position detection, noise and limited precision in the

analog and digital electronics cause substantial drift. In principle, however, our approach can perform feedback based on motion in a second trap, as in Takagi et al. [20]. The design may also be able to perform isotonic experiments, where the trap is manipulated to give a constant error signal relative to itself (and therefore constant load on the microsphere) [21].

Noise and drift

While our noise density for stage-affixed microspheres is comparable to that of Lang et al. [21] at most frequencies, we cannot match their drift or very low frequency performance. Our drift rate of $3.2\ \text{nm/min}$ is nearly an order of magnitude higher than they reported ($<0.5\ \text{nm/min}$) and is due primarily to our use of a non-feedback-controlled microscope stage. This rate of drift is probably representative of most microscope stages

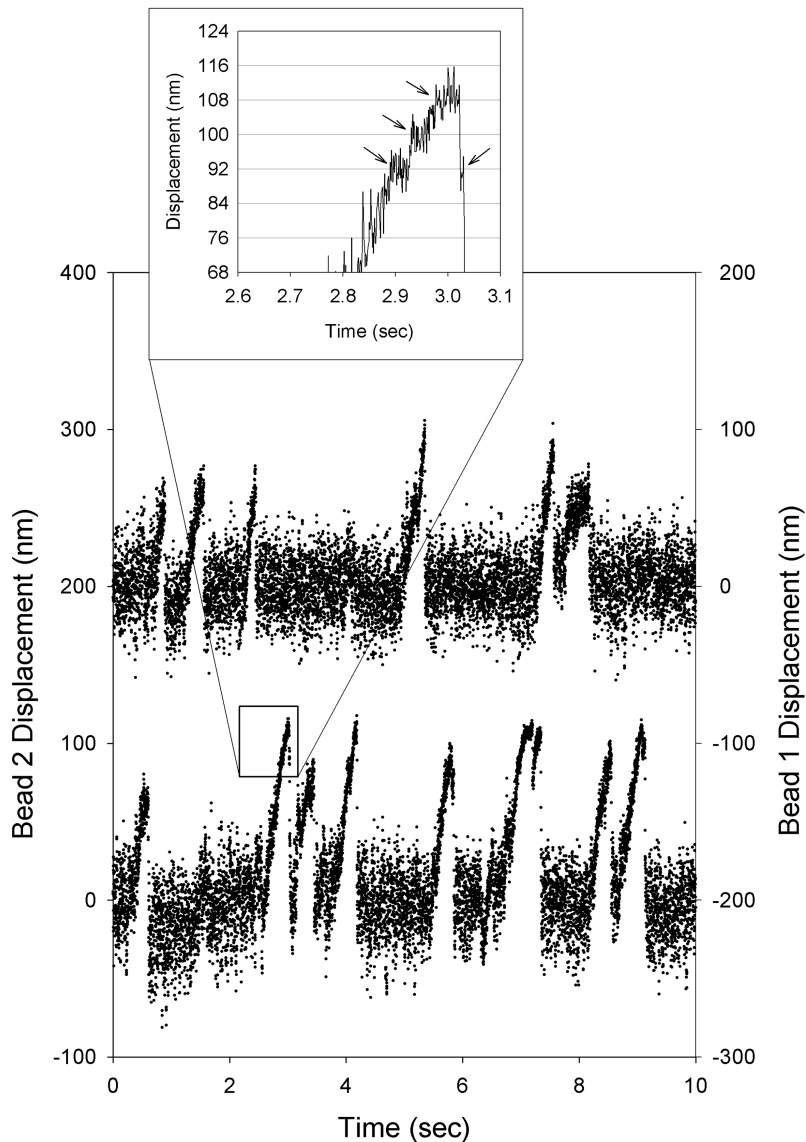


Fig. 5. Single kinesin-mediated displacements of microspheres in two simultaneous laser traps. Two kinesin-coated microspheres were held in separate laser traps and positioned on a common microtubule, approximately $5\ \mu\text{m}$ apart. Kinesin-mediated displacement events are observed simultaneously but asynchronously from both microspheres; 8-nm steps and slips are observed in the low-noise region of each trace. Data shown are Gaussian filtered to 500 Hz. Trap stiffnesses were $0.004\ \text{pN/nm}$.

lacking feedback position control. Our lack of a temperature-controlled, soundproofed room undoubtedly also contributes to drift.

Variations in laser power and pointing stability at frequencies below 1 Hz have been noted by others and attributed to mode hopping in solid-state lasers [13]. Birefringence and hole burning in fiber lasers similarly give rise to low-frequency noise. Birefringence is the property of a material in which the refractive index is polarization dependent. In optical fibers it is induced and altered by mechanical and thermal stress. Mechanical vibrations and variations in the temperature of the fiber therefore induce changes in the polarization of the emitted light. Thus, careful elimination of vibration

sources (e.g., disabling the laser cooling fans) and firmly securing the clad fiber is vital to achieving a stable polarization state.

Hole burning (or polarization hole burning) describes the process by which more gain is partitioned to weaker polarization states in an optical amplifier, such as a fiber laser. This is because stronger polarization components more fully saturate the laser gain, leading to a “redistribution” of gain to weaker polarization components. This is obviously a time-dependent process and explains the random variations in laser power described earlier. We reduced this problem significantly by selecting a polarization apart from the principle polarization axes (see Material and methods). Unfortunately, this only

reduces the variations in power, and does not eliminate them.

This raises the question: with such problems are fiber lasers of any significant benefit in laser traps? For some applications, the answer is yes. Fiber lasers have the benefit of being essentially “instant on” with relatively little warm-up time required. The available energy is exceptional, particularly when considered with regard to “purchase price per watt” (\$5k to \$3k per watt at this writing) and “package size.” Fiber laser sources are very small and are commercially available with CW powers up to 25 W (JPL-Uniphase). The M^2 value of most fiber lasers is 1.0 or perfectly Gaussian to within the limits of measurement. Excellent pointing stability can be achieved. However, while suitable for many single-molecule mechanics studies, because of the low-frequency noise inherent to these lasers, they are not presently suitable when extreme stability is required. Even an inexpensive solid-state laser will typically outperform fiber lasers in power and polarization stability.

Kinesin studies

Kinesin’s step size (8 nm; Svoboda et al. [18]) is well established and determined by the spacing of kinesin binding sites on microtubules. We were easily able to resolve steps and slips at multiples of this fundamental step size. We additionally measured the velocity of unloaded beads along microtubules to be 357 nm/s, which is similar to that reported by others [22]. The step pause time calculated from this velocity and the fundamental step size of kinesin was 22.4 ms, which compares well to the step durations measured directly from laser trap data (21.7 ms). All these measures affirm the resolution of the instrument and the accuracy of the calibration.

Simultaneous monitoring of the activity of several kinesin molecules is of questionable value but was used here because of the well-established step size and unloaded velocity of kinesin. Fields that will most benefit from such an instrument are cellular mechanics, membrane dynamics, and the study of low-duty-cycle molecular motors such as myosin, where multiple laser traps are necessary and simultaneous displacement detection is highly desirable.

Future directions

The modular nature and continual improvement of DSP hardware leaves tremendous room for expansion of capabilities. For example, DSP cards will generally support multiple independent processors. This opens the door for adding DSP processors to handle stage control, real-time filtering, spectral analysis, or other processor-intensive tasks in addition to data collection and laser pointing. The opportunity for moving more I/O capabilities onto industry-standard expansion cards also

exists. These may include on-board DDS for AOD control or higher-resolution A/D conversion than is currently available, which may permit elimination of the analog computer. A distinct advantage here is that modularity allows one to continually expand the capabilities of the system without wholesale redesign of the laser trap components.

Of particular interest is replacing the current A/D IP card with one that would support triggered acquisition of data. While the current A/D card captures data at several times the position switching rate, there is a variable interval between any given position change and the subsequent A/D integration interval. The resulting phase change can result in exaggerated aliasing. Antialiasing filters cannot be used because they would effectively blend together the multiplexed signals from the multiple trap positions. Triggering the acquisition to eliminate phase changes would help to minimize aliasing artifacts.

The PCI chip set on the DSP card used in this project was not capable of direct bus mastering. Direct bus mastering is different from DMA in that a single, initial setup of the addressing allows the DSP card to write into the host memory as though the memory were local. This would reduce what is currently the rate-limiting step in switching laser trap positions—the setup of DMA on each cycle for reading instructions from the host computer and writing data back to the host computer. While this is certainly not necessary to achieve a useful (if not excessive) number of traps, it would allow one to eliminate assembly code from the DSP program, as the added speed would no longer be needed. It would alternatively allow other processing steps to be inserted into the code, such as real-time filtering of data.

The bus architecture that we currently use to add I/O capabilities is the IP standard, with most of our expansion cards mounted on a “carrier board.” The IP standard limits the available selection of I/O expansion modules and limits the bit width of interboard data transfers to 16 bits. As an alternative, VMEbus is a resilient standard with many available expansion modules. Unfortunately, these cards may not be mounted within a standard computer chassis. Rather, VMEbus requires backplane mounting, and the backplane normally runs a real-time OS. This is obviously contrary to the goals of our design. In contrast, the PCI mezzanine card standard allows multiple expansion cards to be mounted to a standard PCI card with fast interboard communications, up to 32 bit transfers, and no OS. In our opinion, this rapidly expanding standard represents a superior choice for future development of DSP-based laser trap control systems.

Acknowledgments

The authors thank Mr. Arun Thomas for his early work on our software, Mr. Bin Guo and Ms. Linda

Rinko for assembly of the analog computer, and Mr. Donald Gaffney of the University of Vermont for many helpful discussions on the limitations of software-based trap control. This work was supported by the Cardiovascular Research Center at the University of Virginia and by grants from the National Institutes of Health (AR45604 and HL64381).

References

- [1] J.T. Finer, R.M. Simmons, J.A. Spudich, Single myosin molecule mechanics: piconewton forces and nanometre steps, *Nature* 368 (1994) 113–119.
- [2] S.M. Block, K. Svoboda, Analysis of high resolution recordings of motor movement, *Biophys. J.* 68 (1995) 2305S–2395S.
- [3] K. Visscher, S.M. Block, Versatile optical traps with feedback control, *Methods Enzymol.* 298 (1998) 460–489.
- [4] W.H. Guilford, D.E. Dupuis, G. Kennedy, J. Wu, J.B. Patlak, D.M. Warshaw, Smooth muscle and skeletal muscle myosins produce similar unitary forces and displacements in the laser trap, *Biophys. J.* 72 (1997) 1006–1021.
- [5] E. Fällman, O. Axner, Design for fully steerable dual-trap optical tweezers, *Appl. Opt.* 36 (1997) 2107–2113.
- [6] J.E. Molloy, Optical chopsticks: digital synthesis of multiple optical traps, *Methods Cell Biol.* 55 (1998) 205–216.
- [7] D.P. Gaffney, A real-time Linux based laser trapping system, in: *Proceedings of the First Joint BMES/EMBS Conference*, p. 875.
- [8] A.D. Mehta, J.T. Finer, J.A. Spudich, Detection of single-molecule interactions using correlated thermal diffusion, *Proc. Natl. Acad. Sci. USA* 94 (1997) 7927–7931.
- [9] C. Veigel, M.L. Bartoo, D.C. White, J.C. Sparrow, J.E. Molloy, The stiffness of rabbit skeletal actomyosin cross-bridges determined with an optical tweezers transducer, *Biophys. J.* 75 (1998) 1424–1438.
- [10] K. Svoboda, S.M. Block, Biological applications of optical forces, *Annu. Rev. Biophys. Biomol. Struct.* 23 (1994) 247–285.
- [11] W.H. Guilford, in: A. Periasami (Ed.), *Methods in Cellular Imaging*, Oxford University Press, New York, 2001, pp. 381–394.
- [12] F. Gittes, C.F. Schmidt, Interference model for back-focal-plane displacement detection in optical tweezers, *Optics Lett.* 23 (1998) 7–9.
- [13] M.W. Allersma, F. Gittes, M.J. deCastro, R.J. Stewart, C.F. Schmidt, Two-dimensional tracking of ncd motility by back focal plane interferometry, *Biophys. J.* 74 (1998) 1074–1085.
- [14] G.J. Wuite, R.J. Davenport, A. Rappaport, C. Bustamante, An integrated laser trap/flow control video microscope for the study of single biomolecules, *Biophys. J.* 79 (2000) 1155–1167.
- [15] A.D. Mehta, J.T. Finer, J.A. Spudich, Reflections of a lucid dreamer: optical trap design considerations, *Methods Cell Biol.* 55 (1998) 47–69.
- [16] W.H. Press, S.A. Teukolsky, W.T. Vetterling, B.P. Flannery, *Numerical Recipes in Pascal*, Cambridge University Press, New York, 1989.
- [17] E. Hamel, A.A. del Campo, M.C. Lowe, C.M. Lin, Interactions of taxol, microtubule-associated proteins, and guanine nucleotides in tubulin polymerization, *J. Biol. Chem.* 256 (1981) 11887–11894.
- [18] K. Svoboda, C.F. Schmidt, B.J. Schnapp, S.M. Block, Direct observation of kinesin stepping by optical trapping interferometry, *Nature* 365 (1993) 721–727.
- [19] W.F. Walker, The significance of correlation in ultrasound signal processing, *Proc. SPIE* 4325 (2001) 159–171.
- [20] Y. Takagi, Y.E. Goldman, H. Shuman, Single molecule force of myosin II measured with a novel optical trap system that eliminates linkage compliance, *Biophys. J.* 78 (2000) 235A.
- [21] M.J. Lang, C.L. Asbury, J.W. Shaevitz, S.M. Block, An automated two-dimensional optical force clamp for single molecule studies, *Biophys. J.* 83 (2002) 491–501.
- [22] S.M. Block, C.L. Asbury, J.W. Shaevitz, M.J. Lang, Probing the kinesin reaction cycle with a 2D optical force clamp, *Proc. Natl. Acad. Sci. USA* 100 (2003) 2351–2356.